Complex Systems **1** (1987) 31–50

Buoyant Mixtures of Cellular Automaton Gases

Christopher Burges
Stéphane Zaleski
Department of Mathematics, Massachussets Institute of Technology, Cambridge, MA 02139, USA

Abstract. The use of lattice gas (cellular automaton) models has recently been advocated as an interesting method for the simulation of fluid flow . These automata are an idealization of the real microscopic molecular dynamics. We present a model derived from the hexagonal lattice gas rules of Frisch Hasslacher and Pomeau (FHP) that incorporates buoyant forces and discusses its properties. We derive the hydrodynamical equations in the low density limit and find the buoyant force and seepage effects characteristic of gravitating mixtures, as well as deviations from the Navier Stokes equations in the compressible case. An equivalent of the quasi-incompressible limit of Boussinesq exists, where the Boussinesq equations are recovered but only for steady flow. The unsteady flow equations suffer from the lack of Galilean invariance of FHP type models. We discuss other tentative models that would overcome this difficulty. The self-diffusion coefficient is also computed from the theory, as well as the mean free path. This allows one to check some of the predictions of the Chapman-Enskog expansion for these gases. We also perform numerical simulations at a Rayleigh number of 6000, showing natural convection near a heated wall and the Rayleigh-Benard instability in a time independent regime.

1. Introduction

Lattice gas models involve an idealization of the physical reality where the molecules are assumed to have discrete positions in space, generally on some regular lattice, and the velocities are also discrete [1]. The purpose of this contribution is to investigate how deterministic lattice gases, or cellular automata, can be used to simulate mixtures of fluids with external, for instance gravitational, forces. Frisch, Hasslacher and Pomeau have introduced models where the velocities of the particles are transformed in collisions in a deterministic way [2] and advocated the use of the automaton for fluid simulations. This makes the lattice gas a cellular automaton [3] . It is in a way a very simplified model of molecular dynamics, and it allows one

to bridge the gap between microscopic and macroscopic physics [4]. This is of course what the kinetic theory of gases purports to do, and the first investigations of the lattice gas were made in that context [6]. The recent interest in lattice gases was stimulated by the discovery that the hexagonal lattice gas or FHP gas obeys the Navier Stokes equations in the large scale limit. This gas is thus of great interest for fundamental investigations of large physical systems, in particular when the physics at the small scales of the motions are complicated and the large scale behavior is not very well understood[1]. Besides this fundamental interest, the lattice gas might be able to compete with finite difference and spectral methods for the simulation of some flows. Its advantages are its programming simplicity, its easy adaptation on parallel processors, and its stability properties.

As an example of the simplicity of the cellular automaton, consider the problem of simulating fluid flow in cavities with very convoluted shapes: the boundaries of those cavities are no more difficult to treat with a cellular automaton than straight walls. The cellular automaton is well adapted to parallel machines with only local communications. This is true of others schemes as well, but in the case of the cellular automaton, it is also likely that one local error would not affect the accuracy of the solution, which is obtained by averaging over many cells. Finally, the cellular automaton is always stable: its state is always close to an equilibrium analogous to the equilibrium state of gases. This state has maximum entropy or H function (see [1] for an introduction to the kinetic theory of lattice gases). The necessity of averaging the motion of the particles, the fault tolerance and the stability all stem from the fact that in the cellular automaton the microscopic disorder of nature is simulated. This latter fact also makes the cellular automaton less efficient than the resolution of Partial Differential Equations (P.D.E.'s) (assuming they exist for the problem of interest) if what is desired is an arbitrary accuracy. However, the situation is different if one wishes to reach larger and larger scales, or Reynolds numbers. The efficiency of the cellular automaton is thus much harder to determine than its programming simplicity[2].

In this paper we do not try to prove that there are problems for which the CA can be more efficient, although we briefly return to this question in the conclusion. We rather would like to explore the ability of the automaton to describe a large variety of physical situations. Can the lattice gas be modified to model buoyancy driven flows, also of great theoretical and practical importance? This contribution is devoted to a preliminary attempt to answer this question. We first define the rules of our automaton, which is best understood as a mixture of two almost identical fluids. Working with

[1] Examples among many are provided by rapid flow in porous media or by multiphase flow

[2] Arguments have been given [8] to the effect that for a given precision, increasing the Reynolds number requires more work as do existing methods of solution of the Navier-Stokes equations. However, as also explained by Orszag and Yakhot [8], if the boundary conditions are of a complicated form the cellular automaton could be more efficient.

$$p_i + p'_{i+3} \overset{1/2}{\longleftrightarrow} p_{i+1} + p'_{i+4}$$
$$p_i + p'_{i+3} \overset{1/2}{\longleftrightarrow} p_{i-1} + p'_{i+2}$$
$$p_i + p'_{i+2} + p''_{i+4} \longleftrightarrow p_i + p'_{-i-2} + p''_{-i-4}$$
$$p_i \overset{g_{P,ij}}{\longrightarrow} p_j$$

Table 1: The first three rules are the rules of the hexagonal FHP gas. The symbols p,p', etc ... denote blue or red particles (r or b). The last line describes the effect of gravity on the particles.

mixtures has many advantages. At this stage the main one is simplicity: as in the FHP model the temperature is not a thermodynamic variable. For our model we show how kinetic theory can be used to predict the large scale behavior of the automaton. We find a set of compressible hydrodynamical equations. In the incompressible, or Boussinesq, limit, these equations are identical to the generally accepted equations when the flow is steady.

The diffusion coefficient has been numerically computed through simulations in the absence of gravity or buoyancy effects. When gravity is added, typical flow structures are seen. For unsteady flow, a modification of the rules is proposed that yields the correct equations in the low density limit. These rules include irreversible collisions, which allows one to explore an interesting new class of models.

2. The lattice gas mixture with external force fields: defining rules

We consider particles that live on the links of a triangular lattice. The particles can be "blue" or "red" and have any of the six unit velocities on the lattice, but there cannot be more than one particle with the same velocity at the same point. The six directions on the lattice, corresponding to unit vectors $\mathbf{c}_0, ..., \mathbf{c}_5$ are labelled counterclockwise with $\mathbf{c}_0 = \mathbf{e}_x$. The particles simply cross each other on nodes, unless one of the collisions described in Table 1 and Figure 1 occurs.

The rules (1),(2),(3) in Table 1 are just the rules of the FHP model, but in addition we specify how particles of different colors are scattered in a collision. Rule (4) introduces buoyant forces by deviating red and blue particles at some sparse locations in space and time. The probability that a particle of color P be deviated from direction i to direction j is denoted $g_{P,ij}$ (Figure 2). Boundary conditions can be free slip, no slip or periodic as in standard lattice gas models. For instance, no slip conditions are obtained by modelling the boundary as a barrier on which particles may only bounce back to the site they come from. One can impose the color of the particles coming away from a collision with the boundary, or impose a rate of change of color at the boundary, simulating fixed concentration or fixed flux con-

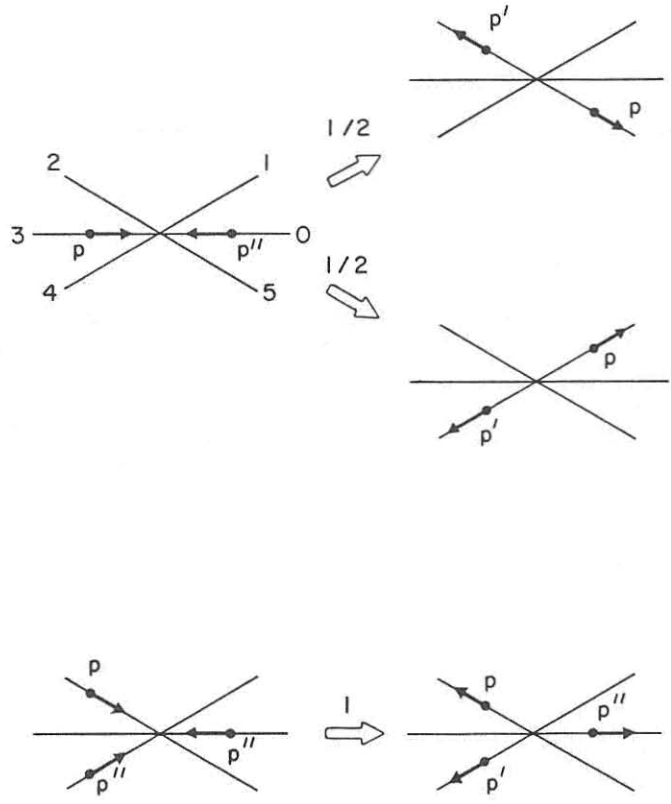

Figure 1: Collision rules for the two color reversible model. The particles colliding head on are deviated to the right or the left every odd or even time step.

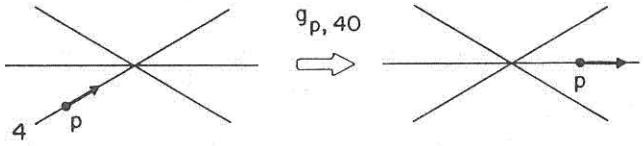

Figure 2: The gravity effect for the reversible model. This effect occurs at preassigned sites.

ditions. Our automaton can thus be most closely compared to a mixture of fluids with identical physical properties but for their susceptibility to external forces. This latter property suggests the analogy with charged particles. However, the "charge" in our model is always so small that the interaction between the particles is vanishing. This is similar to an imaginary world where the inertial mass would not be equal to the gravitational mass. Because in many fluid configurations the only density changes that are relevant are those producing buoyant forces (in the so-called Boussinesq approximation) this change of gravitational mass is the only one relevant at the large scale. We will get to this point after deriving the hydrodynamical equations (hydrodynamical is here synonymous to large scale) from kinetic theory. We first derive approximate equations for the compressible subsonic flow in the CA.

3. The hydrodynamical equations

As in [6] we assume that the gas is ergodic and that ensemble averages correspond to space and time averages at thermodynamic equilibrium. Let $R_i(\mathbf{x},t)$ $(B_i(\mathbf{x},t))$ be the number of red (blue) particles headed in direction i at position x and time t and let $N_i = R_i + B_i$. Let $\mathbf{c}_i$ be the unit vector in the i direction. The index i will always be understood to be modulo 6. There are three independent quantities conserved in the collisions in our model (omitting the effects of gravity):

$$\begin{aligned} \rho &= \textstyle\sum_i N_i \\ \mathbf{p} &= \textstyle\sum_i N_i \mathbf{c}_i \\ R &= \textstyle\sum_i R_i \end{aligned} \tag{3.1}$$

The local velocity $\mathbf{u}$ is defined by $\mathbf{p} = \rho\mathbf{u}$. The conservation of mass can be immediately written as

$$\frac{\partial \rho}{\partial t} + \mathrm{div}\rho\mathbf{u} = 0 \tag{3.2}$$

We assume that the state of the automaton is obtained by patching local equilibrium states. This means that to derive the momentum and color equations we make a Chapman-Enskog expansion of the solutions of the

Boltzmann equation. Although it is not clear whether this procedure is well justified for the cellular automaton, we expect it will have an asymptotic meaning in the low density limit and not too far from equilibrium. The numerical results we give below also partially vindicate this approach for quite high densities.

In our derivation, we assume molecular chaos, which implies that the n-particle distribution functions (DF) that describe the state of the system can be written as products of one-particle DF. It will be convenient to note X the 12-vector $(R_1, B_1, ..., R_6, B_6)$. With this assumption, the time evolution of X can be written as a discrete Boltzmann-like equation[3]

$$\begin{aligned} R_i(\mathbf{x}+\mathbf{c}_i, t+1) - R_i(\mathbf{x}, t)i \\ = \quad & -\sum_j g'_{R,ij} R_j + \Omega(X)_{2i-1}, B_i(\mathbf{x}+\mathbf{c}_i, t+1) - B_i(\mathbf{x}, t) \\ = \quad & -\sum_j g'_{B,ij} B_j + \Omega(X)_{2i}, \end{aligned} \tag{3.3}$$

where

$$g'_{P,ij} = -g_{P,ji} + \sum_k g_{P,jk}\delta_{ij}. \tag{3.4}$$

Thus, a collision like the one of Figure 2 generates two contributions to the Boltzmann equation. The collision operator Ω is defined by:

$$\begin{aligned} \Omega(X)_{2i-1} &= \frac{1}{2}\Lambda(R, i+1; N, i-2) + \frac{1}{2}\Lambda(R, i-1; N, i+2) \\ &- \Lambda(R, i; N, i+3) + \Lambda(R, i+3; N, i-1; N, i+1) \\ &- \Lambda(R, i; N, i+2; N, i+4) \end{aligned} \tag{3.5}$$

with

$$\Lambda(P^{(1)}, i_1; ...; P^{(k)}, i_k) = \frac{P^{(1)}_{i_1}}{1-N_{i_1}} ... \frac{P^{(k)}_{i_k}}{1-N_{i_k}} \prod_{i=1}^{i=6}(1-N_i) \tag{3.6}$$

and where all the DF are estimated at $\mathbf{x}, t$. Identical relations hold for $\Omega(X)_{2i}$ provided B and R are exchanged. To solve the Boltzmann equation, we make a Chapman Enskog expansion, that is, we assume that the system is close to statistical equilibrium and that all conserved quantities vary slowly in space and time. The intensity of the external force effects is also small in the following sense: in the actual computer implementation of the CA, deflections that model the action of external forces occur at sparse locations at the microscopic scale. On the large scale, however, the CA fluid is homogeneous, so that the distribution function behaves as if the deflections occurred everywhere at a very small rate $\max(g_{P,ij})$. We take

[3]Some of the discussion below parallels the one in [5], but for the fact that we start from the truly discrete Boltzman equation. This has some importance for some subtle effects that we discuss below when we compute the viscosity.

the "distinguished limit" where the two small parameters are related by: $\max(g'_{P,ij}) = O(\nabla)$. The Chapman Enskog expansion of the distribution function is then

$$X = X^{(0)} + X^{(1)} + ... + X^{(n)} + ... \tag{3.7}$$

The lowest order has already been given in many references. One only needs to solve:

$$\Omega(X^{(0)}) = 0 \tag{3.8}$$

which can be done quite easily using Fermi Dirac distributions [1]. The result is:

$$P_i^{(0)} = \frac{P}{6}(1 + 2(u.c_i) + 4a(\rho)(u_i^2 - 1/2u^2)) + ... \tag{3.9}$$

where $a(\rho) = (\rho - 3)/(\rho - 6)$ and P is R or B. Higher order approximations (in gradient) are obtained by linearization of the operator Ω around $R^{(0)}$. This expansion allows one to find explicitly that the automaton obeys equations similar to the Navier Stokes equations. Looking for higher order approximations generates a hierarchy of equations of the form:

$$Y^{(n)} = \left.\frac{\delta\Omega}{\delta X}\right|_{X=X^{(n)}} X^{(n+1)} \tag{3.10}$$

where at the first order

$$Y^{(1)} = \partial_t X^{(0)} + DX^{(0)} + GX^{(0)} \tag{3.11}$$

and where DX is the propagation term of the Boltzmann equation:

$$DX = (\mathbf{c}_i.\nabla R, \mathbf{c}_i.\nabla B). \tag{3.12}$$

Gravity is represented by $GX = (\sum g'_{R,ij} R_j, \sum g'_{B,ij} B_j)$. At this point it is convenient to define the scalar product of two 12-vectors $A' = (a'_i)$ and $B' = (b'_i)$:

$$(A'|B') = \sum_{i=1}^{12} a'_i b'_i. \tag{3.13}$$

Equation (11) can be solved only if certain solvability conditions are met, of the form:

$$(Z|Y^{(n)}) = 0 \tag{3.14}$$

where Z is a null eigenvector of $\delta\Omega/\delta X$. The solution of the first order equation is discussed in the appendix. The solvability condition or Fredholm alternative (14) yields at second order:

$$\begin{aligned}
\frac{\partial \rho u_\alpha}{\partial t} &+ \frac{\partial}{\partial x_\beta}(\rho a(\rho) u_\alpha u_\beta) = -\frac{\partial \varpi}{\partial x_\alpha} + g_{1,R\alpha}(u)R + g_{1,B\alpha}(u)B \\
&+ \frac{\partial}{\partial x_\beta}\left(\eta(\rho)/\rho \frac{\partial \rho u_\alpha}{\partial x_\beta}\right) + O(g'_{p,ij}\nabla u) + O(g'^2_{p,ij} u) \\
\frac{\partial \theta}{\partial t} &+ \frac{\partial \theta u_\alpha}{\partial x_\alpha} = \frac{1}{\rho}\frac{\partial}{\partial x_\alpha}\left(D(\rho)\rho \frac{\partial \theta}{\partial x_\alpha} + \mathbf{J_g}(\theta)\right)
\end{aligned} \tag{3.15}$$

where $\varpi = \rho(1-a(\rho)u^2)/2$ is the pressure and $\theta = R/\rho$ is the color fraction. The indices α,β span the two space directions x, y. The intensity of the buoyant forces is represented by the vectors $\mathbf{g_{1,P}}$. They depend only on the interaction coefficients $g'_{P,ij}$ and the velocity $\mathbf{u}$. External forces also create a seepage flow $\mathbf{J}_g(\theta)$. We computed the gravitational force $\mathbf{g_{1,P}}$ and the seepage flow in the low density limit and to first order in the velocity u. It is convenient to express the result in complex form:

$$g_{1,Px}(w) + \mathrm{i}g_{1,Py}(w) = -\frac{1}{6}\sum_{i,j}\left[g'_{P,ij}\xi^i(1+\xi^j w + \overline{\xi}^j\overline{w} + O(w^2))\right] \quad (3.16)$$

$$J_{gx} + \mathrm{i}J_{gy} = -2(\mathbf{g_{1,R}} - \mathbf{g_{1,B}})\theta(1-\theta) + O(w) \quad (3.17)$$

where $w = u_x + \mathrm{i}u_y$ and $\xi = \exp 2\mathrm{i}\pi/6$. In equation (15), η is the shear viscosity, already derived by this method and measured from simulations [7]. The derivation can be found in [5] (see also [9]):

$$\eta(\rho)/\rho = \frac{1}{12f(1-f)^3} - \frac{1}{8} \quad (3.18)$$

where $f = \rho/6$[4]. Although the above equations were derived in the low density limit, we independently computed the diffusion coefficient D for arbitrary densities using the Chapman Enskog expansion:

$$D(\rho) = \frac{1}{f(1-f)^3(3f+1)} - \frac{1}{4}. \quad (3.19)$$

This compares well with the simulations that we report below. A diffusion coefficient is also given in [5]. The rules used in this latter reference are slightly different but the coefficient obtained is consistent with our computations, but for the propagation diffusivity term discussed previously. At this stage, we obtain equations that are similar to the usual fluid equations for a mixture of two non-reacting fluids, but with some additional terms. The fact that the CA is not Galilean invariant is reflected in three different discrepancies with the compressible Navier-Stokes equations: (*i*) in the advective term $a(\rho)$; (*ii*) in the dependence of the pressure and the external force intensity on the local velocity; (*iii*) in the term $\partial_\beta[(\eta/\rho)\partial_\beta(\rho u_\alpha)]$. This term produces additional contributions to the momentum flux of the form $\eta(u_\alpha/\rho)\partial_\beta\rho$. This latter symptom of the "Galilean disease" of the CA [1] seems to have been overlooked by previous workers [9],[7].

Other terms correspond to genuine effects in a real gas mixture. The additional flux term $\mathbf{J}_g(\theta)$ in the color conservation equation tends to bring

[4]The $-1/8$ term does not appear in [5] directly in the formula given for ν but can be deduced from what is called in section 2 of this reference "higher order lattice size corrections". Its origin lies in the discrete character of the lattice and it is also called a propagation viscosity. If one thinks of the flux of colored particles accross a link (it can be written $R_0 - R_3$) the right going particles come from a site at say x but the left going come from a site at $x + c_0$. Thus the populations R_0 and R_3 are not estimated at the same points, and an additional term proportional to $\nabla\theta$ appears in the flux.

the lighter particles above the heavier. This is a relevant effect at atmospheric or astrophysical scales. For convection in a laboratory setting, however, these effects are small. In what follows, we show that there is a corresponding limit for the CA fluid that yields a classical idealization for buoyant fluids.

4. The Boussinesq approximation

An approximation widely used in buoyant flow is to consider the density of the fluid and its material properties as constant except in the gravity force term. This approximation can be shown to result from an asymptotic expansion in some small parameters [10]. The approximation is here made easier because the density ρ does not depend on the color ratio θ. Here we only have to prove that the density is approximately constant. The thermodynamic considerations that arise in the thermal convection problem are also avoided in the CA.

In the buoyant fluid layer, two causes can yield strong variations of the density: (*i*) strong hydrostatic pressure gradient; (*ii*)transonic flow velocities. The hydrostatic gradient is given by :

$$\nabla \ln \rho = \mathbf{g}_{1,B} - (\mathbf{g}_{1,B} - \mathbf{g}_{1,R})\theta \tag{4.1}$$

This suggests introducing a small parameter ϵ:

$$\epsilon^2 = gh, \tag{4.2}$$

where the ratio of the depth h of the fluid layer to the gravitational 'scale height' $1/g$ where $g = |g_{1R} - g_{1B}|$. Case (*i*) is avoided if $\epsilon << 1$. To avoid case ii) , the velocity caused by buoyant forces must be bounded. A very likely bound is the velocity of free fall of a cold fluid lump with maximum buoyancy:

$$V = (2gh\Delta\theta)^{1/2} \tag{4.3}$$

where $\Delta\theta$ is the scale of color ratio variations. Thus the Mach number will remain small if $2\epsilon << 1$. To summarize, the density of the fluid will be approximately constant if $\epsilon << 1/2$. This suggests taking the velocity scale V and the space scale h, and rewriting equations (15). The full procedure, as carried out by [10] in the thermal convection case, involves keeping all the small terms in the equations and expanding the solutions in powers of ϵ. In this short presentation, we simply give the rescaled equations at lowest order in ϵ:

$$\nabla'.v' = O(\epsilon) \tag{4.4}$$

$$\frac{\partial u'}{\partial t'} + u'.\nabla(a(\rho_0)u') = -\nabla'\varpi' + \mathbf{e_y}\theta + \frac{\nu}{g^{1/2}d^{3/2}}\Delta u' + O(\epsilon u) \tag{4.5}$$

$$\frac{\partial \theta}{\partial t'} + u'.\nabla'\theta = \frac{D}{g^{1/2}d^{3/2}}\Delta'\theta + O(\epsilon\theta)) \tag{4.6}$$

where $\nu = \eta/\rho$, $u' = u/V$, $x' = x/d$, $t' = tV/d$. Dropping all the terms of order ϵ yields the classical Oberbeck Boussinesq (OB) equations [11]. It is remarkable that all non Boussinesq terms disappear at small ϵ simultaneously. In addition, taking the small ϵ limit also ensures that the expansion of the one particle distribution function in powers of the Mach number remains valid.

The usual choice in convection theory [12] is to take the Rayleigh number Ra and the Schmidt number σ as the two independent dimensionless numbers. For our model those numbers would be:

$$Ra = \frac{g\Delta\theta h^3}{D\nu}, \qquad \sigma = \nu/D \tag{4.7}$$

However, before the CA can model convection at such values of the parameters, several problems must be solved:

(a) Time dependent motion and stability of stationary motion could be adequately computed only if the advective term $a(\rho_0)$ is set back to 1. A tentative solution to this problem is presented in section 7 of this paper.

(b) The Schmidt number we obtain is rather low, of the order of 1/12 in the low density limit. It can, however, be easily increased by introducing collisions that exchange the color but not momentum, like

$$r_i + b_{i+k} \longleftrightarrow b_i + r_{i+k} \tag{4.8}$$

Assuming these problems are solved, what would be the maximal Rayleigh number in a simulation? For a 2d CA computation with $\epsilon = 0.1$, and $\sigma \simeq 1$, the answer is:

$$Ra_{max} \simeq \frac{h^2}{10\,\nu^2} \tag{4.9}$$

where h is the number of sites in the vertical direction.

5. Numerical investigation of some kinetic properties

We have numerically investigated the diffusion properties of the CA mixture. In all these computations the gravity was set to zero, and there was no large scale momentum. From the assumption of molecular chaos the mean free path can be easily estimated :

$$\lambda_{\mathrm{mfp}} = 1/\lambda_{\mathrm{mfp2}} + 1/\lambda_{\mathrm{mfp3}} \tag{5.1}$$

where

$$\lambda_{\mathrm{mfp2}} = 6/\rho(1-\rho/6)^{-4} \qquad \lambda_{\mathrm{mfp3}} = (6/\rho)^2(1-\rho/6)^{-3} \tag{5.2}$$

These expressions are in good agreement with the measurements. We also measured the diffusion coefficient, using a cavity of size 64×256 with periodic lateral boundaries and rigid upper and lower boundaries. The color was fixed on the upper and lower boundaries. The color fraction profile was

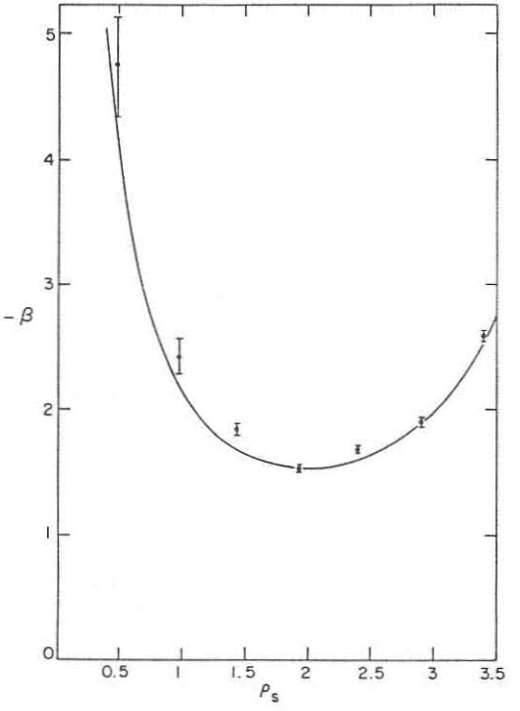

Figure 3: This plot shows measurements of the flux of colored particles in a nonequilibrium situation. The coefficient β is proportional to the number of particles crossing a given plane. The full line shows the prediction of the small gradient expansion, and the measured points were obtained as explained in the text.

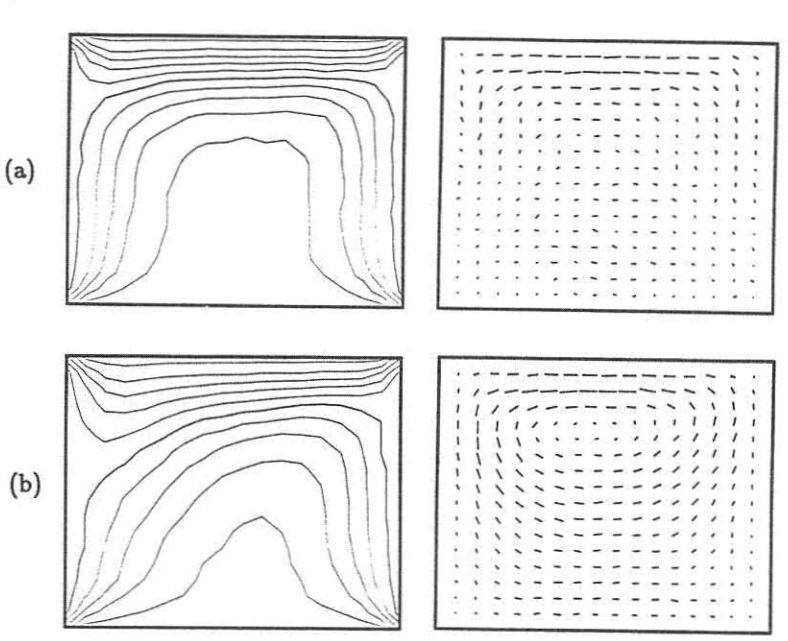

Figure 4: Contour lines for the color ratio and the velocity field in a closed gap with heating from the side. (a) t= 2046; (b) t= 4000.

found to be linear except for the lowest density measurements, where the mean free path was a large fraction of the total size. The color flux was measured at several heights. This yields an estimate of the dependency of the flux on the color gradient: $X^{(1)}_{2j-1} = \beta/2\nabla\theta\xi^j + c.c.$ in the absence of density or momentum gradient. We plot the numerical result for β along with the theoretical prediction (consistent with (19)) on figure 3.

6. Flow simulations

We used the model described above to simulate fluid flow. The gravity kicks occurred every time step at preselected sites of the automaton. These sites were regularly spaced, and we took care to maintain the "scale height" parameter ϵ small enough. We used a Sun-3 which gave a speed of about 50 000 site updates per second. The density was always set to 1 and the scale height parameter ϵ was set to 0.2. This results in a Schmidt number about 0.13. In the first simulation, a square box 1024×1024 was used with four rigid walls. The left wall was blue or "cold" while the right one was red or "hot". The conditions on the bottom and top walls amounted to fix the color ratio to $\theta = 1/2$. The evolution of the flow is shown on figure 4.

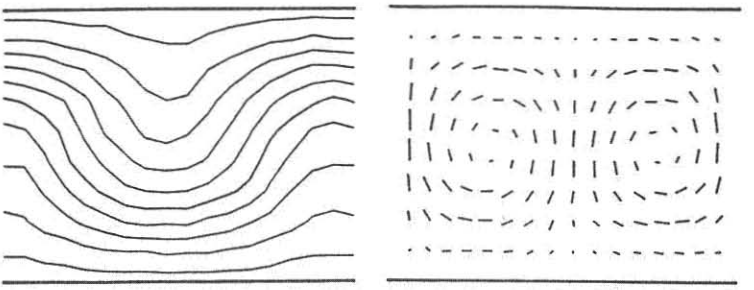

Figure 5: Benard instability. The instability was initiated by a small perturbation near the cell center. The circulation is rapidly created

The characteristic circulation is a well known phenomenom that occurs at any Rayleigh number. In this case the Rayleigh number based on the box size was about 6000.

In the second simulation the box was periodic in the horizontal dimension while the upper, rigid, plate was cold and the lower was hot. The box was of size 512×1024 and the Rayleigh number was also about 6000. We have seen the Rayleigh-Benard instability develop as shown on figure 5. Its amplitude grows rapidly as expected in a low Prandtl number fluid and the Mach number reaches 0.3 in 4000 time steps. These simulations show that convective fluid flow is indeed realizable with cellular automaton fluids. Further simulations are in progress on faster machines and should allow one to treat more difficult situations such as complicated boundary conditions.

7. Pseudo Galilean invariance in irreversible models

The model with have worked with so far has the serious flaw that the velocity advection term $a(\rho)u \cdot \nabla u$ is different from the true term in the Euler equations. A method that allows one to restore the correct value of that term is presented below. It has the interesting property of involving rules which are not reversible, i.e., for each collision configuration the configuration obtained by changing the arrow of time does not necessarily produce a collision. In this new model we introduce center particles, which are particles resting motionless on a lattice site. These particles may be red or blue but only one is allowed at each site. They normally collide with the other particles in the same way as in the models with centers introduced by FHP [2]. However the collisions that create those particles are not symmetrical

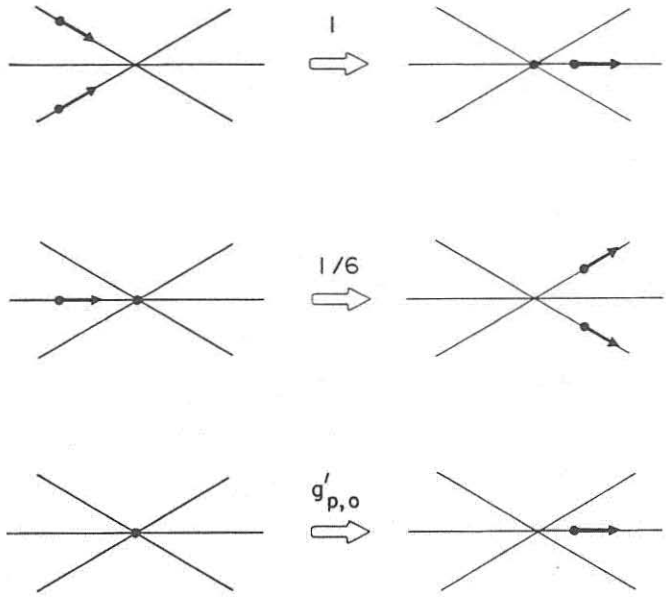

Figure 6: Collision rules for the irreversible model. The two first diagrams show the irreversible collisions on centers. The last diagram indicates how gravity is implemented in this model.

with those which destroy them: see figure 6. Also, the gravity kicks can now be imposed only on centers, making the effect more symmetrical. The probability of creating a center is always one, while the probability of destroying it is α'. As a result a steady state is obtained where there are more centers than in the reversible models.

An interesting situation occurs in the low density limit when one sets $\alpha' = 1/6$. To explain the derivation of the new hydrodynamical equations, we first redefine the fundamental quantities: we let R_i, B_i be as before the distribution of moving particles for $i = 0, 5$ and R_7, B_7 be the distribution of centers. We define ρ and u as above, and ρ_c be the density of center particles. R and B are as above the density of red and blue particles, including the centers. Then for vanishing ρ we find that the lowest order in the Chapman- Enskog expansion is, at third order in u:

$$R_i = \frac{R}{12}(1 + 4\mathbf{u}.\mathbf{c}_i + 8\mathbf{u}.\mathbf{c}_i - 2u^2)R_6 = \frac{R}{2}(1 - 2u^2) \qquad (7.1)$$

with analogous expressions for the blue particles. It is seen that half of the particles are centers in the zero velocity state. Proceeding as in the previous case, we obtain the hydrodynamical equations. Computations are similar to those of the appendix but with 14-vectors. We find equations identical to the hydrodynamical equations above, but with $a(\rho) = 1 + O(\rho)$. Thus the Euler equations are Galilean invariant for our model , although it is not Galilean invariant at the microscopic scale. This is what we call pseudo Galilean invariance. The pressure is now $\varpi = \rho/4$, which can be easily understood by the fact that only half of the particles, the moving ones, contribute to the pressure. We find a shear viscosity $\eta = 3/7$, compression viscosity $\xi = 3/28$ and a color diffusivity $D = 6/5$. The color diffusivity is clearly smaller than in the reversible case. This can be easily explained if one notices that there are now many more possible collisions, which reduces the mean free path.

The velocity of sound is now $c_s = 1/2$, but contrarily to the reversible case, it will now depend on the density. The steady state in the absence of momentum can be easily obtained for any density and the velocity of sound so deduced fits well with numerical simulations communicated to us by D. Rothman .

We thus have to caution that the results obtained for the irreversible models might depend strongly on the density. In particular, the pseudo Galilean invariance is lost for $\rho = 1$. Another problem could be the lack of stability of the steady state. The stability of the equilibrium state in the reversible case is generally proved through the Boltzmann H theorem, as shown by Hénon [13]. However, the proof requires reversibility and cannot be extended to this model. This appears not to be a problem in low density as all the eigenvalues of the Boltzmann operator are negative or zero and all the diffusivities are positive. These latter facts are necessary for stability.

8. Conclusion

We have presented a lattice gas model that yields large scale equations similar to the Boussinesq equations, but for the coefficients of the nonlinear terms. The model is much simpler than models with several velocities and requires interactions between nearest neighbors only. The equations obeyed by the model can be obtained by kinetic theory and the derivation of diffusivity coefficient is consistent with the results of direct numerical simulations. Preliminary simulations allow one to see typical buoyancy driven flows. The model thus appears to be a reliable tool for the study of moderate Rayleigh number flow. It is, however, necessary to increase the complexity of the model in order to restore Galilean invariance. This is done using a nonreversible model which is shown to yield a stable steady state.

We believe that the state reached so far by the lattice gas theory does not render justice to its enormous potential applications. The possibility of having very simple models of the microscopic physics should allow one to simulate many phenomena that cannot be attained by macroscopic equations or are not obtained very efficiently. Many complicated phenomena of this type exist in mixtures, for instance problems with separation of components, surface tension and impurities. The work done so far should provide a basis for the development of more complicated models.

9. Acknowledgements

The authors wish to thank P. Lallemand, C.C. Lin, W.V.R Malkus, B. Hasslacher, and Y. Pomeau for their encouragement and advice and for many fruitful conversations. Special thanks go to D. Rothman for providing data on the sound velocity in the irreversible model. C. Burges was supported in part by NSF grant 8407109-PHY and Department of Energy Contract No DE-AC-02-76 ERO 3069. S. Zaleski was supported in part by NSF grant No DMS-8603752 and benefited from a NATO grant for international travel nr 85/0509.

Appendix A. Inversion of the linearized Boltzmann operator

We look for a solution of equation (10) at the first order, in terms of the conserved quantities $R, \rho, \mathbf{u}$. We represent those solutions as vectors $X = (R_1, B_1, ..., R_6, B_6)$. The linearized Boltzmann operator can be written at lowest order in $\mathbf{u}$ and ρ:

$$\frac{\delta \Omega}{\delta X}|_{X=X^{(0)}} = \Omega' \qquad (A.1)$$

where

$$\Omega' = \frac{1}{12}\begin{pmatrix} -2\rho & 0 & \rho & 0 & R & R & -2R & -2R & R & R & \rho & 0 \\ 0 & -2\rho & 0 & \rho & B & B & -2B & -2B & B & B & 0 & \rho \\ \rho & 0 & \ddots & & & & & & & & & \\ 0 & \rho & & \ddots & & & & & & & & \\ R & R & & & \ddots & & & & & & & \\ B & B & & & & \ddots & & & & & & \\ -2R & -2R & & & & & \ddots & & & & & \\ -2B & -2B & & & & & & \ddots & & & & \\ R & R & & & & & & & \ddots & & & \\ B & B & & & & & & & & \ddots & & \\ \rho & 0 & & & & & & & & & \ddots & \\ 0 & \rho & & & & & & & & & & \ddots \end{pmatrix} \tag{A.2}$$

Notice that the upper row of two by two blocks is reproduced at each level, only shifted by two positions. This is a result of rotational invariance. The missing elements are easily deduced by noticing this fact. The right eigenvectors of Ω' are defined by

$$\Omega' Z_i = \lambda_i Z_i \tag{A.3}$$

and are

$$Z_i = (R, B, \xi_i R, \xi_i B, ..., \xi_i^5 R, \xi_i^5 B) \tag{A.4}$$

where $\xi_k = \exp(2i\pi k/6)$, and

$$Z_{i+6} = (1, -1, \xi_i, -\xi_i, ..., \xi_i^5, -\xi_i^5) \tag{A.5}$$

Similarly, the left eigenvectors of Ω' are

$$Z_i^\dagger = (1, 1, \xi_{-i}, \xi_{-i}, ..., \xi_{-i}^5, \xi_{-i}^5) Z_{i+6}^\dagger = (B, -R, B\xi_{-i}, -R\xi_{-i}, ..., B\xi_{-i}^5, -r\xi_{-i}^5) \tag{A.6}$$

and the eigenvalues are

$$\lambda_i = -2\rho + \xi\rho + \xi^2\rho - 2\rho\xi - 2\rho\xi^3 + \rho\xi^4 + \rho\xi^5 \lambda_{i+6} = -2\rho + \rho(\xi + \bar{\xi}) \tag{A.7}$$

There are four zero eigenvalues, corresponding to invariant conservation: mass, color and momentum, plus a spurious zero eigenvalue (λ_3). The spurious eigenvalue is a result of the fact that in the low density limit we consider only two particle collisions. These collisions conserve momentum line by line and thus preserve additional invariants. To carry out the calculations in the low density limit we require an additional condition:

$$(Z_3^\dagger | Y^{(1)}) = 0 \tag{A.8}$$

This is verified if $g_R^{(3)} = g_B^{(3)} = 0$, where we use the reduced rates:

$$g_P^{(n)} = \sum_{i,j} g'_{P,kj} \xi^k \tag{A.9}$$

The linearized Boltzmann equation (3) can now be solved using the general formula:

$$X^{(1)} = \sum_{\lambda_i \neq 0} \frac{(Z_i^\dagger | Y^{(1)})}{(Z_i^\dagger | Z_i)} Z_i \tag{A.10}$$

The result is best expressed as a sum of two terms:

$$X^{(1)} = X_a^{(1)} + X_b^{(1)} \tag{A.11}$$

where

$$X^{(1)}_{2j-1,a} = \frac{R\xi^{2j}}{6\rho^2}(2\bar{g}_R^{(2)} R + 2\bar{g}_B^{(2)} B - 3\partial_{\bar{z}}\rho w) + c.c. + \mathcal{O}(\partial_t w) \tag{A.12}$$

and $c.c.$ stands for complex conjugate. $X^{(1)}_{2j,a}$ is obtained by exchanging R and B in the above expression. Also

$$X^{(1)}_{2j-1,b} = \frac{\xi^j}{3}[(\bar{g}_{1,R} - \bar{g}_{1,B})\theta(1-\theta) - 3\partial_{\bar{z}}\theta] + \frac{\xi^{2j}}{9}[(\bar{g}_{2R} - \bar{g}_{2B})\theta(1-\theta) - 3\rho w \partial_{\bar{z}}\theta] + c.c. + \mathcal{O}(\partial_t w) \tag{A.13}$$

$$\text{and} \qquad X^{(1)}_{2j,b} = -X^{(1)}_{2j-1,b} \tag{A.14}$$

Writing the linearized Boltzmann equation (10) at next order order, we obtain

$$Y^{(2)} = \partial_t X^{(1)} + DX^{(1)} + GX^{(1)} + \frac{1}{2}D^{(2)}X^{(0)} + \frac{1}{2}\partial_{t^2}^2 X^{(0)} + \partial_t D X^{(0)}. \tag{A.15}$$

The hydrodynamical equations are now obtained as as the solvability condition for this equation. The momentum conservation is represented by the equation:

$$(Z_1^\dagger | Y^{(1)} + Y^{(2)}) = 0. \tag{A.16}$$

To write the color conservation equation, it is useful to define the null eigenvector $Z'^\dagger = (1, -1, ..., 1, -1)$. Then (14) implies

$$(Z'^\dagger | Y^{(1)} + Y^{(2)}) = 0 \tag{A.17}$$

It is not necessary to take all the terms in equation (15) into account. The first term on the r.h.s. $\partial_t X^{(1)}$ disappears in all the scalar products. The next term is of order $1/\rho$ and dominates all the others in the low density limit. If one wishes to find all the relevant terms outside the low density limit, they must be investigated one by one. A quick check yields the result that all these terms provide contributions which are of higher order in Mach number, so that it is consistent to neglect them as we have already made an expansion in small u. Equations (16) and (17) can then be simplified into

$$(Z_1^\dagger | Y^{(1)} + DX^{(1)}) = 0 \tag{A.18}$$

and

$$(Z'^\dagger | Y^{(1)} + DX^{(1)}) = 0 \tag{A.19}$$

This yields the hydrodynamical equations (15) of the text.

References

[1] R. Gatignol, *Theorie cinetique des Gaz a repartition discrete des vitesses*, (Springer, New York, 1975).

[2] U. Frisch, B. Hasslacher and Y. Pomeau, *Physical Review Letters* **56** (1986) 1505.

[3] J. Salem and S. Wolfram, "Thermodynamics and Hydrodynamics with Cellular Automata" in *Theory and Applications of Cellular Automata*, edited by S. Wolfram (World Scientific, 1986).

[4] N. Margolus, T. Toffoli and G. Vichniac, *Physical Review Letters*

[5] S. Wolfram, *Journal of Statistical Physics*, **45** (1986) 471-526.

[6] J. Hardy and Y. Pomeau, *Journal of Mathematical Physics* **13** (1972) 1042; J. Hardy, O. de Pazzis and Y. Pomeau, *Journal of Mathematical Physics* **14**, (1973) 1746; J. Hardy, O. de Pazzis and Y. Pomeau, *Physical Review A* **13** (1976) 1949.

[7] D. D'Humieres, P. Lallemand and T. Shimomura, "An experimental study of lattice gas hydrodynamics", submitted to *Physical Review Letters.*

[8] V. Orszag and V. Yakhot, *Physical Review Letters* **56** (1986) .

[9] J.P. Rivet and U. Frisch,*Comptes Rendus Acad. Sc. Paris II*, **302** (1986) 267.

[10] E.A. Spiegel and G. Veronis, *Astrophysical Journal* **131**, (1960) 442-447.

[11] J. Boussinesq, *Theorie analytique de la chaleur*, volume 2, page 172 (Gauthier Villars, Paris, 1903).

[12] R.P. Behringer, *Review of Modern Physics*, (July 1985); F.H. Busse, *Reports on Progress in Physics* **41** (1978).

[13] M. Henon, unpublished.